Low- and high-energy spectroscopy of ^{17}O and ^{17}F within a microscopic multiphonon approach

G. De Gregorio,[1,2] F. Knapp,[3] N. Lo Iudice,[1,2] and P. Veselý[4]

[1]*Dipartimento di Fisica, Università di Napoli Federico II, 80126 Napoli, Italy*
[2]*INFN Sezione di Napoli, 80126 Napoli, Italy*
[3]*Faculty of Mathematics and Physics, Charles University, 116 36 Prague, Czech Republic*
[4]*Nuclear Physics Institute, Czech Academy of Sciences, 250 68 Řež, Czech Republic*

The extension of an equation of motion phonon method to odd nuclei is described step by step. Equations of motion are first constructed and solved to generate an orthonormal basis of correlated n-phonon states ($n = 0,1,2,\ldots$), built of constituent Tamm–Dancoff phonons, describing the excitations of a doubly magic core. Analogous equations are then derived within a subspace spanned by a valence particle coupled to the n-phonon core states and solved iteratively to yield a basis of correlated orthonormal multiphonon particle-core states. The basis so constructed is used to solve the full eigenvalue problem for the odd system. The formalism does not rely on approximations but lends itself naturally to simplifying assumptions, as illustrated by its application to ^{17}O and ^{17}F. Self-consistent calculations using a chiral Hamiltonian in a space encompassing up to three-phonon basis states generate spectra having a high level density, comparable to that observed experimentally. The spectroscopic properties are investigated at low energy through the calculation of moments, electromagnetic and β-decay transition strengths, and at intermediate and high energy through the computation of the electric-dipole spectra and pygmy and giant dipole resonance cross sections. The analysis of the particle-phonon composition of the eigenfunctions contributes to clarify the mechanism of excitation of levels and resonances and gives unique insights into their nature.

I. INTRODUCTION

The particle-vibration coupling (PVC) model is the most popular approach adopted to determine the corrections by the core excitations to the single-particle energies. The core excitations were described in the past within macroscopic collective models [1] or, microscopically, in the random-phase approximation (RPA) [2].

In recent years, more refined approaches, extending in some cases RPA, were developed within the framework of the energy density functional (EDF) theory. Different functionals were adopted for this purpose. Many of them were derived from Skyrme forces [3–10] or were based on the theory of finite Fermi systems [11]. Others were deduced from relativistic meson-nucleon Lagrangians within the covariant relativistic mean-field framework which describes the core vibrations in the relativistic RPA or the time-blocking approximation [12–15].

Several recent calculations have directly used bare or effective interactions. A Gogny potential was used to evaluate the perturbative contribution of the core excitations, described in RPA, to quadrupole and magnetic moments of several odd nuclei with a valence nucleon external to a magic core [10]. A microscopic quasiparticle model (MQPM) was formulated to evaluate spectra and to study β-decay properties of chains of heavy isotopes [16]. The quasiparticle-phonon model (QPM) was adopted to study the influence of ground-state correlations combined with the Pauli principle on the spectroscopic properties of odd nuclei far from closed shells [17]. Ground-state correlations were also investigated in an extension of the RPA formalism to odd nuclei [18].

Several calculations using bare nucleon-nucleon (NN) plus three-nucleon ($3N$) interactions were performed in several

approaches. An equation of motion method (EOM) rooted within the coupled cluster (CC) theory was specifically developed for studying bulk properties and low-lying spectra of light and medium odd-mass nuclei [19–23]. Most of the CC numerical applications used $NN + 3N$ chiral forces. Analogous interactions were adopted in a self-consistent Green's function theory approach [24], a no-core shell model (NCSM) [25], and a many-body perturbation theory calculation [26].

We have recently extended to odd nuclei [27] an equation of motion phonon method (EMPM) formulated for even-even nuclei [28–30]. In even systems, the EMPM derives a set of equations yielding a basis of orthonormal multiphonon states, built of phonons obtained in the particle-hole (p-h) Tamm–Dancoff approximation (TDA), and then solves the full eigenvalue problem in the space spanned by such a basis.

The method was mainly adopted to investigate the dipole response in heavy neutron-rich nuclei [31–33] in a space including up to two phonons. More recently, it was formulated in a Hartree–Fock–Bogoliubov (HFB) quasiparticle scheme and employed to study the full spectrum as well as the dipole response of neutron-rich ^{20}O [34].

In its extension to odd nuclei [27], an analogous set of equations is derived and solved iteratively to generate an orthonormal basis of states composed of a valence particle coupled to n-phonon states ($n = 1,2,\ldots,n,\ldots$), also generated within the EMPM, describing the excitations of a doubly magic core. The basis is then adopted to solve the full eigenvalue problem. A numerical application to ^{17}O has illustrated the potential of the method.

Here, we describe the formalism in greater detail by going through the different steps leading to the final eigensolutions, specify how it is implemented numerically, and investigate

thoroughly the spectroscopic properties of ^{17}O and ^{17}F at low and high energy.

The same nuclei were investigated in a restricted shell-model calculation embedded in the continuum by using a phenomenological interaction [35]. Energies and widths of a few low-lying states of these $A = 17$ isobars were already determined by an EOM-CC calculation employing a chiral interaction at next-to-next-to-next leading order (N^{3}LO) and a Hartree–Fock (HF) basis coupled to the continuum [20]. In ^{17}O, the pygmy (PDR) and giant (GDR) electric-dipole resonances were explored in a shell-model calculation using the empirical WB10 interaction [36] and performed in the $\{0p,(sd),(pf)\}$ model space up to $3\hbar\omega$ [37].

We adopt a HF basis derived from a chiral NN potential at next-to-next leading order optimized (NNLO$_{\text{opt}}$) so as to minimize the contribution of the three-body term [38]. This potential, while producing too much attraction in medium- and heavy-mass nuclei, reproduces well the experimental binding energies of light nuclei and oxygen isotopes. Thus, we will not add any corrective term as we did for heavy nuclei [33].

Upon solving the equations of motion, we produce a basis of states composed of a valence particle coupled to a full set of TDA phonons generated in a large configuration space plus a subset of two- and three-phonon states, the latter obtained by an approximate procedure which will be described later.

The solution of the eigenvalue problem in a space spanned by the multiphonon basis so derived yields the full set of eigenvalues and eigenstates allowed by the space dimensions. It is thus possible to compare the theoretical level schemes with the full experimental spectra of the two nuclei and to explore in detail their low-lying spectroscopic properties through the calculation of momenta and transition strengths. Finally, the calculation of the electric-dipole strength distribution enables us to investigate the damping and fragmentation of the GDR and the structure of the PDR. By analyzing the phonon composition of the states it is possible to gain a deep insight into the excitation mechanism and to catch the nature of levels and resonances.

II. A BRIEF OUTLINE OF THE METHOD

Let us consider the Hamiltonian

$$H = H_0 + V, \tag{1}$$

where

$$H_0 = \sum_r [r]^{1/2} \epsilon_r (a_r^\dagger \times b_r)^0, \tag{2}$$

and

$$V = -\frac{1}{4} \sum_{rstq\Omega} [\Omega]^{1/2} V_{rstq}^\Omega [(a_r^\dagger \times a_s^\dagger)^\Omega \times (b_t \times b_q)^\Omega]^0. \tag{3}$$

In the above formulas, $a_r^\dagger = a_{x_r j_r m_r}^\dagger$ $[b_r = (-)^{j_r + m_r} a_{x_r j_r -m_r}]$ creates (annihilates) a particle of energy ϵ_r and V_{rstq}^Ω is an unnormalized and antisymmetrized two-body matrix element. The notation $[r]$ stands for $[r] = 2j_r + 1$ and the symbol $\times$ denotes angular-momentum coupling.

It is useful for our purposes to write the two-body potential in the recoupled form

$$V = \frac{1}{4} \sum_{rsqt\sigma} [\sigma]^{1/2} F_{rsqt}^\sigma [(a_r^\dagger \times b_s)^\sigma \times (a_q^\dagger \times b_t)^\sigma]^0 \tag{4}$$

obtained by the use of the Pandya transformation

$$F_{rsqt}^\sigma = \sum_\Omega [\Omega] (-)^{r+t-\sigma-\Omega} W(rsqt; \sigma\Omega) V_{rqst}^\Omega, \tag{5}$$

where $W(rsqt; \sigma\Omega)$ are Racah coefficients.

A. Generation of n-phonon basis

We need to generate first a basis of n-phonon correlated states of the form

$$|\alpha_n\rangle = \sum_{\lambda\alpha_{n-1}} C_{\lambda\alpha_{n-1}}^{\alpha_n} |(\lambda \times \alpha_{n-1})^{\alpha_n}\rangle$$

$$= \sum_{\lambda\alpha_{n-1}} C_{\lambda\alpha_{n-1}}^{\alpha_n} \{O_\lambda^\dagger \times |\alpha_{n-1}\rangle\}^{\beta_n}, \tag{6}$$

where

$$O_\lambda^\dagger = \sum_{ph} c_{ph}^\lambda (a_p^\dagger \times b_h)^\lambda \tag{7}$$

is the p-h TDA phonon operator acting on the $(n-1)$-phonon basis states $|\alpha_{n-1}\rangle$, assumed to be known. As illustrated in Ref. [30], we start with the equations of motion

$$\langle \alpha_n || [H, O_\lambda^\dagger] || \alpha_{n-1}\rangle = (E_{\alpha_n} - E_{\alpha_{n-1}}) X_{\lambda\alpha_{n-1}}^{\alpha_n}, \tag{8}$$

where

$$X_{\lambda\alpha_{n-1}}^{\alpha_n} = \langle \alpha_n || O_\lambda^\dagger || \alpha_{n-1}\rangle = \sum_{\lambda'\alpha_{n-1}'} \mathcal{D}_{\lambda\alpha_{n-1}\lambda'\alpha_{n-1}'}^{\alpha_n} C_{\lambda'\alpha_{n-1}'}^{\alpha_n}, \tag{9}$$

and

$$\mathcal{D}_{\lambda\alpha_{n-1}\lambda'\alpha_{n-1}'}^{\alpha_n} = \langle (\lambda \times \alpha_{n-1})^\beta | (\lambda' \times \alpha_{n-1}')^\beta\rangle \tag{10}$$

is the overlap or metric matrix which reintroduces the exchange terms among different phonons and, therefore, re-establishes the Pauli principle.

After expanding the commutator, expressing the p-h operators in terms of the phonon operators $O_\lambda^\dagger$ upon inversion of Eq. (7), and exploiting Eq. (9), we obtain [30]

$$\sum_{\lambda'\alpha_{n-1}'} (\mathcal{A}\mathcal{D})_{\lambda\alpha_{n-1}\lambda'\alpha_{n-1}'}^{\alpha_n} C_{\lambda'\alpha_{n-1}'}^{\alpha_n} = E_{\alpha_n} \sum_{\lambda'\alpha_{n-1}'} \mathcal{D}_{\lambda\alpha_{n-1}\lambda'\alpha_{n-1}'}^{\alpha_n} C_{\lambda'\alpha_{n-1}'}^{\alpha_n}, \tag{11}$$

where $\mathcal{A}^{\alpha_n}$ is a matrix of the simple structure

$$\mathcal{A}_{\lambda\alpha_{n-1}\lambda'\alpha_{n-1}'}^{\alpha_n} = (E_\lambda + E_{\alpha_{n-1}}) \delta_{\lambda\lambda'} \delta_{\alpha_{n-1}\alpha_{n-1}'} + \mathcal{V}_{\lambda\alpha_{n-1}\lambda'\alpha_{n-1}'}^{\alpha_n}, \tag{12}$$

and $\mathcal{V}_{\lambda\alpha_{n-1}\lambda'\alpha_{n-1}'}^{\alpha_n}$ is a phonon-phonon potential [30].

This is a generalized eigenvalue equation in the overcomplete basis $|(\lambda \times \alpha_{n-1})^{\alpha_n}\rangle$. Following the procedure outlined in Refs. [28,29], based on the Cholesky decomposition method, we extract a basis of linearly independent states

spanning the physical subspace and obtain a nonsingular eigenvalue equation whose solution yields a basis of orthonormal correlated n-phonon states of the form (6).

Since recursive formulas hold for all quantities entering $\mathcal{A}$ and $\mathcal{D}$, it is possible to solve the eigenvalue equations iteratively starting from $n = 1$ (TDA phonons) and thereby generate a set of orthonormal multiphonon states $\{|0\rangle, |\alpha_1\rangle (=|\lambda\rangle), \ldots, |\alpha_n\rangle, \ldots\}$.

The diagonalization of the Hamiltonian in such a multiphonon space yields correlated eigenstates, including the ground state. This is a linear combination of the HF vacuum and of the states $|\alpha_n\rangle$ describing the excitations of fully interacting np-nh configurations. Our approach, in fact, is equivalent to a large-scale shell model in a space spanned by many p-h configurations. In this respect, it differs from RPA and its extensions, where noninteracting np-nh ground-state correlations are accounted for effectively and in quasiboson approximation.

B. Eigenvalue problem in odd nuclei

For a valence nucleon external to a doubly magic the basis states $|v_n\rangle$ of spin v have the form [27]

$$|v_n\rangle = \sum_{p\alpha_n} C_{p\alpha_n}^{v_n} |(p \times \alpha_n)^v\rangle = \sum_{p\alpha_n} C_{p\alpha_n}^{v_n} \{a_p^\dagger \times |\alpha\rangle\}^v, \quad (13)$$

where an odd particle p is coupled to an n-phonon core state of the form (6).

To generate such a basis we started [27] with the equations

$$\langle \alpha_n \| [b_p, H]^p \| v_n \rangle = (E_{v_n} - E_{\alpha_n}) X_{p\alpha_n}^{v_n}, \quad (14)$$

where E_{v_n} are the eigenvalues to be determined and

$$X_{p\alpha}^{v_n} = \langle \alpha_n \| b_p \| v_n \rangle. \quad (15)$$

A procedure analogous to the one adopted for even nuclei leads to the generalized eigenvalue equation

$$\sum_{p'\alpha_n' p''\alpha_n''} \left\{ (\epsilon_p + E_{\alpha_n} - E_{v_n}) \delta_{pp'} \delta_{\alpha_n \alpha_n'} + \mathcal{V}_{p\alpha_n p'\alpha_n'}^v \right\}$$
$$\times \mathcal{D}_{p'\alpha_n' p''\alpha_n''}^v C_{p''\alpha_n''}^v = 0, \quad (16)$$

where $\mathcal{V}_{p\alpha_n p'\alpha_n'}^{v_n}$ is the particle-phonon potential and $\mathcal{D}_{p\alpha_n p'\alpha_n'}^v = \langle (p \times \alpha_n)^v | (p' \times \alpha_n')^v \rangle$ the overlap matrix which reintroduces the exchange terms among the odd particle and the n-phonon states and thereby re-establishes the Pauli principle. The expression of both quantities can be found in Ref. [27].

Following the same procedure adopted for even nuclei, based on the Cholesky decomposition method, we have extracted from the over-complete set $|(p \times \alpha_n)^v\rangle$ a basis of linearly independent states and obtain a nonsingular eigenvalue equation. Its iterative solution, starting from $n = 1$, yields the particle-core states $|v_n\rangle$ (13) of energies E_{v_n} for $n = 1, 2, \ldots$, which, together with the single-particle states $|v_0\rangle$, form an orthonormal basis.

We have now all the ingredients necessary for solving the eigenvalue problem in the full space spanned by $\{|v_0\rangle, |v_1\rangle, \ldots, |v_n\rangle, \ldots\}$:

$$\sum_{v_{n'}} \left\{ (E_{v_n} - \mathcal{E}_v) \delta_{v_n v_{n'}} + \mathcal{V}_{v_n v_{n'}}^v \right\} \mathcal{C}_{v_{n'}}^v = 0, \quad (17)$$

where the matrix elements of $\mathcal{V}$ are nonvanishing for $n' = n \pm 1$ and $n' = n \pm 2$ and have the structure

$$\mathcal{V}_{v_n v_{n'}}^v = [v]^{-1/2} \sum_{p\alpha_n p'\alpha_{n'}} C_{p\alpha_n}^{v_n} \mathcal{V}_{p\alpha_n p'\alpha_{n'}}^v X_{p'\alpha_{n'}}^{v_{n'}}. \quad (18)$$

The expressions of the particle-phonon interactions $\mathcal{V}_{p\alpha_n p'\alpha_{n'}}^v$ are given in Ref. [27].

Equation (17) yields all the eigenvalues allowed by the space dimensions. The eigenfunctions have the structure

$$|\Psi_v\rangle = \sum_{v_n} \mathcal{C}_{v_n}^v |v_n\rangle = \sum_{p\alpha_n} \mathcal{C}_{p\alpha_n}^v |(p \times \alpha_n)^v\rangle, \quad (19)$$

where $\mathcal{C}_{p\alpha_n}^v = \sum_{v_n} \mathcal{C}_{v_n}^v C_{p\alpha_n}^{v_n}$, having made use of Eq. (13).

The procedure leading to this result does not rely on any approximation. It has the same accuracy of shell model. In fact, the Pauli principle is fulfilled and the interaction among valence particles and phonons as well as among phonons is fully taken into account. On the other hand, the particle-phonon scheme allows naturally for reliable and useful approximations.

C. Transition amplitudes

In the coupled scheme, the multipole operator has the structure

$$\mathcal{M}(\lambda\mu) = \frac{1}{[\lambda]^{1/2}} \sum_{rs} \langle r \| \mathcal{M}_\lambda \| s \rangle (a_r^\dagger \times b_s)_\mu^\lambda. \quad (20)$$

Using the wave functions (19), we get the transition amplitudes

$$\langle \psi_{v'} \| \mathcal{M}(\lambda) \| \psi_v \rangle = \sum_{nn'} \mathcal{M}_{nn'}^{(vv')}(\lambda), \quad (21)$$

where

$$\mathcal{M}_{nn'}^{(vv')}(\lambda) = \sum_{v_n v_{n'}'} \mathcal{C}_{v_n}^v \mathcal{C}_{v_{n'}'}^{v'} \langle v_{n'}' \| \mathcal{M}(\lambda) \| v_n \rangle. \quad (22)$$

If the initial and/or final states have dominant single-particle character we can safely use the truncated formula

$$\langle \psi_{v'} \| \mathcal{M}(\lambda) \| \psi_v \rangle \simeq \mathcal{M}_{00}^{(vv')}(\lambda) + \mathcal{M}_{01}^{(vv')}(\lambda) + \mathcal{M}_{10}^{(vv')}(\lambda), \quad (23)$$

where $\mathcal{M}_{00}^{(vv')}(\lambda)$, $\mathcal{M}_{01}^{(vv')}(\lambda)$, and $\mathcal{M}_{10}^{(vv')}(\lambda)$ are, respectively, the particle-particle, particle-phonon, and phonon-particle transition amplitudes, given by

$$\mathcal{M}_{00}^{(vv')}(\lambda) = \sum_{pp'} \mathcal{C}_p^v \mathcal{C}_{p'}^{v'} \langle p' \| \mathcal{M}_\lambda \| p \rangle, \quad (24)$$

$$\mathcal{M}_{01}^{(vv')}(\lambda) = \sum_{pk} \mathcal{C}_p^v \mathcal{M}_{\lambda_k} P_{p\lambda_k}^{(v')}, \quad (25)$$

$$\mathcal{M}_{10}^{vv'}(\lambda) = (-)^{v-v'} \mathcal{M}_{01}^{v'v}(\lambda). \quad (26)$$

$\mathcal{M}_{\lambda_k}$ are the amplitudes of the transitions to the kth TDA state having spin $J_k = \lambda$. They are given by

$$\mathcal{M}_{\lambda_k} = \langle k\lambda \| \mathcal{M}(\lambda) \| 0 \rangle = \frac{1}{[\lambda]^{1/2}} \sum_{ph} c_{ph}^{(\lambda_k)} \langle p \| \mathcal{M}_\lambda \| h \rangle. \quad (27)$$

These amplitudes are weighted by

$$P_{p\lambda_k}^{(\nu')} = \sum_{\nu'_1} \mathcal{C}_{\nu'_1}^{\nu'} X_{p\lambda_k}^{\nu'_1}, \qquad (28)$$

$$P_{p'\lambda_k}^{(\nu)} = \sum_{\nu_1} \mathcal{C}_{\nu_1}^{\nu} X_{p'\lambda_k}^{\nu_1} \qquad (29)$$

in the particle-phonon ($\mathcal{M}_{01}$) and phonon-particle ($\mathcal{M}_{10}$) transitions, respectively. $P_{p\lambda_k}^{(\nu')}$ ($P_{p'\lambda_k}^{(\nu)}$) incorporate the joint contributions of the one-phonon components $|\nu'_1\rangle$ ($|\nu_1\rangle$) of the final (initial) states $|\Psi_{\nu'}\rangle$ ($|\Psi_\nu\rangle$) and of the λ-multipole particle-phonon configurations $|[p \times \lambda_k]^{\nu'_1}\rangle$ ($|[p' \times \lambda_k]^{\nu_1}\rangle$) present in $|\nu'_1\rangle$ ($|\nu_1\rangle$).

III. CALCULATION DETAILS

We used the intrinsic Hamiltonian

$$H = T_{\text{int}} + V_{NN}, \qquad (30)$$

where

$$T_{\text{int}} = \frac{1}{2m} \sum_i p_i^2 - T_{\text{c.m.}} \qquad (31)$$

is the intrinsic kinetic operator and $V_{NN} = \text{NNLO}_{\text{opt}}$ is the *NN* optimized chiral potential derived in Ref. [38] by fixing the coupling constants at next-to-next leading order through a new optimization method in the analysis of the phase shifts, which minimizes the effects of the three-nucleon force. It can be written in the more standard form

$$H = T + V, \qquad (32)$$

where

$$T = \left(1 - \frac{1}{A}\right) \frac{1}{2m} \sum_i p_i^2 \qquad (33)$$

is a modified one-body kinetic term and

$$V = V_{NN} + T_2 \qquad (34)$$

includes the two-body kinetic term

$$T_2 = -\frac{1}{2mA} \sum_{i \neq j} \vec{p}_i \cdot \vec{p}_j. \qquad (35)$$

The above Hamiltonian was employed to generate the HF basis in a space encompassing all harmonic oscillator (HO) shells up to $N_{\max} = 15$. A subset of the HF states so obtained, spanning a space of dimensions corresponding to twelve major shells, was used to determine the TDA phonon basis.

Following the prescription discussed in Ref. [40], we removed from the $J^\pi = 1^-$ TDA phonons the spurious components induced by the center of mass (c.m.) motion by a Gramm–Schmidt orthogonalization of the p-h basis to the c.m. state. This was defined as

$$|\lambda_1\rangle = \frac{1}{N_1} R_\mu |0\rangle = \frac{1}{N_1} \sum_{ph} c_{ph}^{\lambda_1} |(p \times h^{-1})^{1^-}\rangle, \qquad (36)$$

where R_μ is the c.m. coordinate, $c_{ph}^{\lambda_1}$ are the unnormalized coefficients

$$c_{ph}^{\lambda_1} = \sqrt{\frac{4\pi}{9}} \frac{1}{A} \langle p \| r Y_1 \| h \rangle, \qquad (37)$$

and N_1 is the normalization constant

$$N_1^2 = \sum_{ph} \left| c_{ph}^{\lambda_1} \right|^2. \qquad (38)$$

The basis states $|\Phi_i\rangle$ obtained by such an orthogonalization procedure are linear combinations of the p-h states $|(p \times h^{-1})^{1^-}\rangle$. They were used to construct and diagonalize the Hamiltonian matrix yielding eigenstates rigorously free of spurious admixtures. These eigenstates recover the standard TDA structure given by Eq. (7) once the states $|\Phi_i\rangle$ are expressed in terms of the original p-h configurations $|(p \times h^{-1})^{1^-}\rangle$.

The multiphonon basis is composed of all one-phonon particle-core states $|(p \times \alpha_1)^\nu\rangle$, the $|(p \times \alpha_2)^\nu\rangle$ of two-phonon energies $E_{\alpha_2} \leqslant 35$ MeV, and the $|(p \times \alpha_3)^\nu\rangle$ of energies $\epsilon_p + E_{\alpha_3} \leqslant 55$ MeV.

We had to make several approximations in order to include the three phonons. We ignored the interaction $\mathcal{V}_{p\alpha_3 p'\alpha'_3}^{(\nu)}$ in the eigenvalue equation (16) and neglected the phonon-phonon potential ($\mathcal{V}_{\lambda\alpha,\lambda'\alpha'}^\beta = 0$) in Eq. (11) determining the core states $|\alpha_3\rangle$. Furthermore, we neglected in the eigenvalue equation (16) the exchange terms between the odd particle and the phonons and put $\mathcal{D}_{(p\alpha_3)(p'\alpha'_3)}^{(\nu)} \simeq \delta_{pp'}\delta_{\alpha_3\alpha'_3}$. Under these approximations, the three-phonon eigenstates are simply $|\nu_3\rangle \sim |(p \times \alpha_3)^\nu\rangle$ and the couplings (18) become

$$\mathcal{V}_{\nu_n \nu_3}^\nu = \sum_{pp'\alpha_n} C_{p\alpha_n}^{\nu_1} \mathcal{V}_{p\alpha_n p'\alpha_3}^\nu. \qquad (39)$$

The lack of antisymmetrization between the odd particle and $|\alpha_3\rangle$ in $|(p \times \alpha_3)^{\nu_3}\rangle$ may yield some linear dependence among these states and might overestimate their couplings to the one-phonon and two-phonon particle-core components. The other two approximations affect the energy distribution of states lying at high energies and, therefore, do not have appreciable consequences.

IV. SPECTRA AND PHONON COMPOSITION OF WAVE FUNCTIONS

The theoretical spectra obtained for ^{17}O and ^{17}F are compared to one another and with experiments in Fig. 1. At high energies, the density of levels is comparable with or higher than the experimental one in both nuclei. The low-energy spectra, instead, are less dense, especially in ^{17}O.

To get useful insights into the nature of the levels, it is useful to investigate the effect of the different phonon subspaces and the structure of the wave functions.

A. ^{17}O

The action of the different phonon subspaces was discussed in Ref. [27]. By inducing a depression of the lowest $5/2_1^+$, the particle-phonon coupling brings most of the low-lying levels of single-particle nature closer to the experimental ones. No new
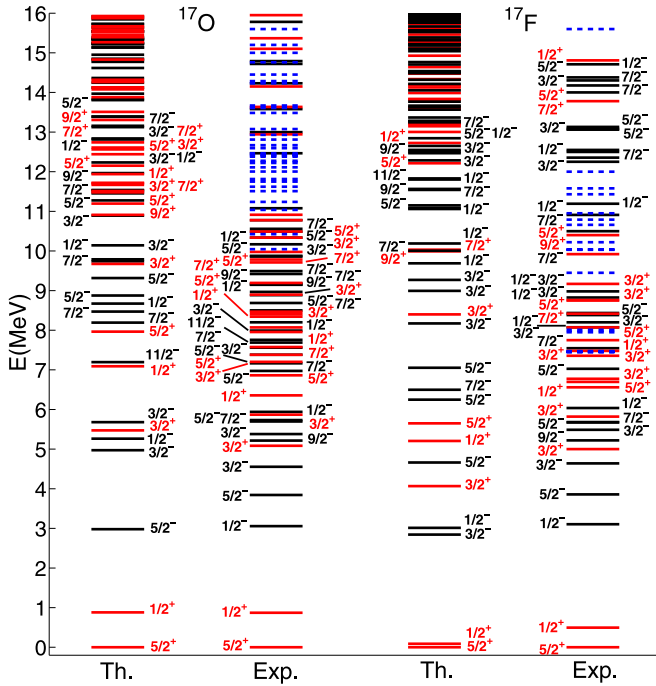
FIG. 1. Theoretical versus experimental [39] spectra of ^{17}O and ^{17}F. The dashed levels have unknown spin or parity or both.

TABLE I. Phonon composition of selected states $|\Psi_\nu\rangle$ [Eq. (19)] in ^{17}O.

J_π^ν	E^ν	$|C_0^\nu|^2$	$|C_1^\nu|^2$	$|C_2^\nu|^2$	$|C_3^\nu|^2$
$\frac{5}{2}^+_1$	0.0000	0.9510	0.0484	0.0005	0.0001
$\frac{1}{2}^+_1$	0.8808	0.9408	0.0586	0.0002	0.0004
$\frac{5}{2}^-_1$	2.9796	0.0003	0.7500	0.0120	0.2377
$\frac{3}{2}^-_1$	4.9733	0.8855	0.0942	0.0021	0.0182
$\frac{1}{2}^-_1$	5.2635	0.9787	0.0198	0.0001	0.0014
$\frac{3}{2}^+_1$	5.4730	0.9457	0.0535	0.0004	0.0004
$\frac{3}{2}^-_2$	5.6798	0.0969	0.7137	0.0185	0.1709
$\frac{1}{2}^+_2$	7.0899	0.9710	0.0247	0.0001	0.0002
$\frac{11}{2}^-_1$	7.1942	0.0006	0.8822	0.0752	0.0420
$\frac{5}{2}^+_2$	7.9645	0.9862	0.0128	0.0002	0.0008
$\frac{7}{2}^-_1$	8.1929	0.4278	0.4856	0.0195	0.0671
$\frac{1}{2}^-_2$	8.4706	0.0171	0.8459	0.0108	0.1262
$\frac{7}{2}^-_2$	8.6719	0.1446	0.7575	0.0350	0.0629
$\frac{5}{2}^-_2$	8.8762	0.3692	0.5663	0.0336	0.0309
$\frac{5}{2}^-_3$	9.3157	0.6084	0.3481	0.0231	0.0204
$\frac{9}{2}^+_1$	10.9115	0.0074	0.8290	0.0944	0.0692
$\frac{5}{2}^+_3$	11.1951	0.0067	0.8545	0.0208	0.1180
$\frac{3}{2}^+_3$	11.4801	0.0075	0.8534	0.0108	0.1283
$\frac{9}{2}^-_1$	11.5319	0.0005	0.9342	0.0345	0.0308
$\frac{7}{2}^+_1$	11.9392	0.0081	0.8449	0.0680	0.0790
$\frac{9}{2}^+_3$	13.3058	0.0175	0.5434	0.4057	0.0334

levels, however, occur in the low-energy spectrum. The one-phonon particle-core states, in fact, fall at energies $\gtrsim$11 MeV and increment greatly the level density of the high-energy spectrum. The low-energy region is not affected by the two phonons, either. These components contribute to enrich further the high-energy sector.

Only the three phonons are able to push a few states, all of negative parity, down in energy and, therefore, modify the low-energy spectrum. This, however, remains much less dense than the experimental low-energy-level scheme.

As shown in Table I, the low-energy intruders, of negative parity, have a dominant one-phonon character and, in a few cases, mix strongly single-particle and particle-phonon components. All low-lying positive-parity states have single-particle nature.

At high energies ($E \gtrsim 11$ MeV), most of the states of both parities have dominant one-phonon components. States combining one- and two-phonon pieces appear at $E \gtrsim 13$ MeV. Those of dominant two-phonon character are at higher energies ($E \gtrsim 16$ MeV).

The different impact of two- and three-phonon states was established already for ^{16}O [29,30] and can be understood by observing that the coupling between one and three phonons is intimately correlated with the zero-phonon to two-phonon coupling through the formula

$$\langle\alpha_3|V|\alpha_1\rangle = \sum_{\alpha_2}\langle\alpha_3|(\alpha_1 \times \alpha_2)^{\alpha_3}\rangle\langle\alpha_2|V|0\rangle. \qquad (40)$$

One should therefore expect that such a coupling is strong since the HF vacuum is strongly coupled to two phonons.

The one-phonon to two-phonon coupling is, in general, not sufficiently strong to affect the low-energy phonons. It is

more effective in the high-energy sector where one and two phonons have comparable energies and, therefore, mix with one another, as shown in Table I.

The two phonons couple strongly to four phonons as indicated by the formula

$$\langle\alpha_4|V|\alpha_2\rangle = \sum_{\beta_2}\langle\alpha_4|(\alpha_2 \times \beta_2)^{\alpha_4}\rangle\langle\beta_2|V|0\rangle. \qquad (41)$$

One should, therefore, expect the occurrence of low-energy intruders of dominant two-phonon nature and of mixed phonon structure as a result of such a strong coupling.

The different behavior of states of different parities may be traced back to the HO constituents of the HF states. The HF p-h configurations are built of p-h HO states, whose energies are $(2n + 1)\hbar\omega$ and $(2n + 2)\hbar\omega$ ($n = 0, 1, 2, \ldots$) for negative and positive parity, respectively. Correspondingly, the negative-parity phonons have in general lower energies than the corresponding phonons of positive-parity. Several three-phonon states are composed entirely of negative-parity phonons and, therefore, have lower energies as well. Also an appreciable number of positive-parity two-phonon states composed of two negative-parity phonons lie at relatively low energies. Only if coupled to four phonons, however, would these states have intruded into the low-energy sector. Unfortunately, the four phonons are not included in our calculation.

TABLE II. Weights W_λ^ν [Eq. (42)] of the one-phonon components of selected states $|\Psi_\nu\rangle$ in ^{17}O.

		$W_\lambda^\nu \times 10^2$							
	λ	1^-	2^-	3^-	4^-	1^+	2^+	3^+	4^+
ν									
^{17}O	$\frac{5}{2}^+_1$	0.3	0.4	0.5	0.2	0.4	0.8	0.6	0.4
	$\frac{1}{2}^+_1$	0.6	0.6	0.5	0.1	0.9	1.2	0.6	0.2
	$\frac{5}{2}^-_1$	12.9	14.6	21.5	10.2	4.1	6.0	1.1	0.7
	$\frac{3}{2}^-_1$	2.9	2.6	1.7	0.4	0.4	0.4	0.2	0.1
	$\frac{1}{2}^-_1$	0.6	0.4	0.4	0.0	0.1	0.1	0.0	0.0
	$\frac{3}{2}^+_1$	0.5	0.6	0.5	0.2	0.9	1.0	0.5	0.3
	$\frac{3}{2}^-_2$	23.5	19.8	12.1	3.0	3.4	2.8	1.5	0.6
	$\frac{1}{2}^+_2$	0.2	0.2	0.2	0.0	0.4	0.5	0.2	0.1
	$\frac{11}{2}^-_1$	0.2	0.2	86.8	0.6	0.0	0.2	0.1	0.3
	$\frac{5}{2}^+_2$	0.0	0.1	0.1	0.0	0.2	0.3	0.1	0.0
	$\frac{7}{2}^-_1$	10.7	5.6	24.8	3.9	0.3	1.1	0.6	0.4
	$\frac{1}{2}^-_2$	25.2	16.5	23.4	0.5	3.8	2.3	1.3	0.5
	$\frac{7}{2}^-_2$	11.1	6.0	52.6	2.3	0.4	1.1	0.6	0.6
	$\frac{5}{2}^-_2$	3.7	3.9	46.4	1.6	0.5	0.6	0.3	0.2
	$\frac{5}{2}^-_3$	3.0	3.5	24.6	0.2	0.3	0.4	0.2	0.1
	$\frac{9}{2}^+_1$	2.3	0.7	60.1	0.3	0.3	12.9	0.0	3.7
	$\frac{5}{2}^+_3$	0.3	2.5	13.0	0.5	17.7	33.7	9.8	1.2
	$\frac{3}{2}^+_3$	6.3	1.8	9.9	0.2	21.8	30.1	11.2	0.7
	$\frac{9}{2}^-_1$	0.0	8.3	84.6	0.1	0.1	0.1	0.1	0.1
	$\frac{7}{2}^+_1$	0.4	1.4	0.9	0.2	33.2	37.0	2.1	0.2

The different multipoles enter the one-phonon components $|(p \times \lambda)^\nu\rangle$ of the total wave functions $|\Psi_\nu\rangle$ with weights

$$W_\lambda^\nu = \sum_p W_{p\lambda}^\nu, \qquad (42)$$

where

$$W_{p\lambda}^\nu = \frac{1}{[v]^{1/2}} \sum_{k\nu_1} |\mathcal{C}_{\nu_1}^\nu|^2 C_{p\lambda_k}^{\nu_1} X_{p\lambda_k}^{\nu_1}. \qquad (43)$$

This formula is deduced from inserting the expansion of the bra $\langle\Psi_\nu|$ in terms of n-phonon components into the normalization condition

$$\langle\Psi_\nu|\Psi_\nu\rangle = \sum_{\alpha_n} W_{\alpha_n}^\nu = 1. \qquad (44)$$

As Table II indicates, all multipoles are present with comparable small weights in the states of single-particle nature. As for the states with dominant phonon components, all odd multipoles contribute with comparable weights to most negative-parity states while few of them have a full octupole character. The octupole components are dominant also in few positive-parity states like $9/2_1^+$. The even multipoles are all present in the positive-parity states with an overall predominance of the quadrupole components.

B. ^{17}F

The coupling to the one-phonon space has a strong impact also on the HF level scheme of ^{17}F (Fig. 2). As in ^{17}O, it acts more strongly on the $5/2_1^+$ state thereby promoting the inversion between the $1/2_1^+$ and $5/2_1^+$ levels. The correct ground state is thus obtained. The $1/2_1^+$ level, however, is only ~100 keV above $5/2_1^+$ and about ~300 keV below the corresponding experimental level.

Due to the more pronounced depression of the $5/2_1^+$ state, the other low-lying levels appear at higher energies in better overall agreement with the experiments.

The particle-phonon levels are at too high energies and enhance greatly the level density only in that region. The two-phonon components increment further the density in the high-energy sector but affect marginally the low-lying level scheme.

In analogy with ^{17}O, the strongest effect is produced by the coupling to the three-phonon subspace which pushes a few negative-parity levels down in the low-lying spectrum, although not in sufficient number to approach closely the experimental level scheme. In fact, two or three loopholes appear in the theoretical level scheme which originate from the much larger gaps of the HF spectrum. Apparently the phonon coupling is not strong enough to wipe them out.

As in ^{17}O, most of the intruders have particle-phonon nature, while few are linear combinations of HF and particle-phonon states (Table III). All negative-parity multipole components are present in these states with comparable amplitudes. Only few high-spin states have a dominant octupole nature (Table IV).

No positive-parity particle-core states intrude into the low-energy spectrum (Table III). In fact, only positive-parity levels of single-particle nature with small phonon admixtures occur at low energy. Consequently, the amplitudes of all the different multipoles entering these states are very small (Table IV).

Positive-parity states of one-phonon or two-phonon nature or characterized by a mixture of both components appear at high energies. The quadrupole components prevail in several states (Table IV).

V. MOMENTS AND TRANSITIONS

A. Magnetic moments and β-decay ft value

For the magnetic-dipole operator

$$\vec{\mu} = \sum_k (g_l(k)\vec{l}_k + g_s(k)\vec{s}_k), \qquad (45)$$

we used bare gyromagnetic factors, $g_l(k) = 1$ and $g_s(k) = 5.59$ for protons, $g_l(k) = 0$ and $g_s(k) = -3.83$ for neutrons.

We also computed for the ground-state β decay of ^{17}F the ft value

$$ft_{1/2} = \frac{\kappa}{B_F + B_{GT}}, \qquad (46)$$

where $\kappa = 6146$ s. The reduced strengths are

$$B_F(i \to f) = \frac{1}{[J_i]}|\langle f, J_f \| \mathcal{M}_F \| i, J_i\rangle|^2,$$

$$B_{GT}(i \to f) = \frac{1}{[J_i]}|\langle f, J_f \| \mathcal{M}_{GT} \| i, J_i\rangle|^2, \qquad (47)$$
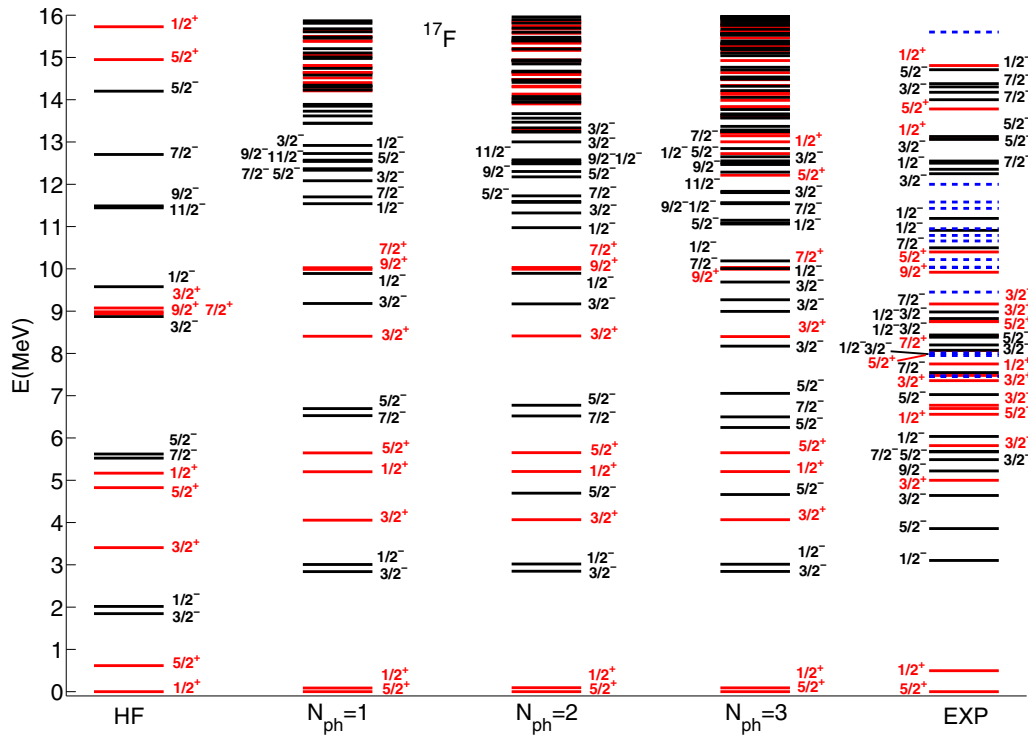
FIG. 2. Level schemes of ^{17}F determined in different multiphonon spaces. N_{ph} denotes the maximum phonon number.

TABLE III. Phonon composition of selected states $|\Psi_\nu\rangle$ in ^{17}F.

J_π^ν	E^ν	$|C_0^\nu|^2$	$|C_1^\nu|^2$	$|C_2^\nu|^2$	$|C_3^\nu|^2$
$\frac{5}{2}^+_1$	0.0000	0.9647	0.0351	0.0002	0.0000
$\frac{1}{2}^+_1$	0.0892	0.9675	0.0323	0.0001	0.0001
$\frac{3}{2}^-_1$	2.8437	0.9899	0.0098	0.0001	0.0002
$\frac{1}{2}^-_1$	3.0131	0.9897	0.0100	0.0000	0.0003
$\frac{3}{2}^+_1$	4.0666	0.9796	0.0203	0.0000	0.0001
$\frac{5}{2}^-_1$	4.6630	0.0215	0.7483	0.0220	0.2082
$\frac{1}{2}^+_2$	5.2050	0.9721	0.0277	0.0001	0.0001
$\frac{5}{2}^-_2$	6.2479	0.3456	0.4573	0.1710	0.0261
$\frac{7}{2}^-_1$	6.4988	0.9740	0.0244	0.0008	0.0008
$\frac{5}{2}^-_3$	7.0536	0.6353	0.2550	0.0888	0.0209
$\frac{3}{2}^-_2$	8.1726	0.0009	0.8486	0.0157	0.1348
$\frac{3}{2}^+_2$	8.3989	0.9447	0.0546	0.0002	0.0005
$\frac{3}{2}^-_3$	8.9938	0.4756	0.4722	0.0086	0.0436
$\frac{1}{2}^-_2$	9.6875	0.5268	0.4416	0.0032	0.0284
$\frac{9}{2}^+_1$	9.9913	0.9859	0.0137	0.0003	0.0001
$\frac{7}{2}^-_2$	10.0064	0.0053	0.9278	0.0335	0.0334
$\frac{7}{2}^+_1$	10.0325	0.9866	0.0131	0.0002	0.0001
$\frac{1}{2}^-_3$	10.1882	0.4312	0.5326	0.0043	0.0319
$\frac{7}{2}^-_3$	11.1503	0.4717	0.4972	0.0169	0.0142
$\frac{9}{2}^-_1$	11.5656	0.0030	0.9400	0.0300	0.0270
$\frac{11}{2}^-_1$	11.8336	0.0061	0.8985	0.0510	0.0444

TABLE IV. Weights W_λ^ν of the one-phonon components of selected states $|\Psi_\nu\rangle$ in ^{17}F.

		$W_\lambda^\nu \times 10^2$							
ν	λ	1^-	2^-	3^-	4^-	1^+	2^+	3^+	4^+
^{17}F	$\frac{5}{2}^+_1$	0.2	0.3	0.3	0.2	0.3	0.6	0.4	0.3
	$\frac{1}{2}^+_1$	0.3	0.2	0.2	0.1	0.5	0.6	0.4	0.2
	$\frac{3}{2}^-_1$	0.2	0.2	0.1	0.0	0.0	0.0	0.0	0.0
	$\frac{1}{2}^-_1$	0.2	0.2	0.2	0.0	0.0	0.0	0.0	0.0
	$\frac{3}{2}^+_1$	0.2	0.2	0.1	0.0	0.3	0.4	0.2	0.1
	$\frac{5}{2}^-_1$	14.0	16.7	23.5	6.9	2.4	3.5	1.5	0.1
	$\frac{1}{2}^+_2$	0.3	0.2	0.2	0.0	0.5	0.5	0.3	0.1
	$\frac{5}{2}^-_2$	8.8	11.4	9.6	3.4	2.7	3.1	2.4	1.1
	$\frac{7}{2}^-_1$	0.5	0.3	0.8	0.3	0.0	0.1	0.1	0.1
	$\frac{5}{2}^-_3$	4.8	6.1	5.6	2.3	1.3	1.7	1.2	0.5
	$\frac{3}{2}^-_2$	34.9	27.1	12.7	2.9	1.6	1.5	0.9	0.3
	$\frac{3}{2}^+_2$	0.4	0.6	0.4	0.1	1.0	1.1	0.6	0.4
	$\frac{3}{2}^-_3$	28.2	8.3	4.6	2.4	0.9	0.8	0.4	0.2
	$\frac{1}{2}^-_2$	18.1	15.1	6.9	0.2	1.0	0.7	0.3	0.1
	$\frac{7}{2}^-_2$	4.2	4.5	76.8	5.5	0.1	0.6	0.2	0.3
	$\frac{7}{2}^-_3$	13.2	5.9	20.7	5.0	0.3	1.8	0.7	0.8
	$\frac{9}{2}^-_1$	0.2	3.6	88.8	0.6	0.1	0.1	0.1	0.1
	$\frac{11}{2}^-_1$	0.7	0.4	85.1	1.2	0.0	0.5	0.1	0.5

TABLE V. Ground-state magnetic μ (μ_N) and electric-quadrupole Q (efm^2) moments, $B(E\lambda; J_i^\pi \to J_f^\pi)$ $(e^2 fm^{2\lambda})$ and ft value. The experimental data are taken from Ref. [39]. The sign of the experimental quadrupole moment of ^{17}F is not known.

		HF	EMPM	Expt.
^{17}O	μ	-1.91	-1.83	-1.89
	Q	0	-0.841	-2.578
	$B(E2; 5/2_1^+ \to 1/2_1^+)$	0	0.17	2.18(16)
	$B(E1; 5/2_1^+ \to 5/2_1^-)$	0.0083	0.0042	0.0004
	$B(E1; 1/2_1^+ \to 1/2_1^-)$	0.482	0.249	0.0005
	$B(E1; 1/2_1^+ \to 1/2_2^-)$	0.0173	0.0005	
^{17}F	μ	$+4.79$	$+4.63$	$+4.72$
	Q	-9.9	-7.6	5.8(4)
	$B(E2; 5/2_1^+ \to 1/2_1^+)$	40.71	21.89	21.64
	$B(E1; 5/2_1^+ \to 5/2_1^-)$	0.015	0.0004	0.0018
	$B(E1; 1/2_1^+ \to 1/2_1^-)$	0.60	0.40	0.0006
	$B(E1; 1/2_1^+ \to 1/2_2^-)$	0.0087	0.0265	
	$B(E1; 1/2_1^+ \to 1/2_3^-)$	0.0000	0.0013	
	$\log ft$	3.294	3.391	3.358(2)

where the Fermi and Gamow–Teller operators are

$$\mathcal{M}_F = g_v \sum_k t_+(k), \qquad (48)$$

$$\mathcal{M}_{GT} = g_A \sum_k t_+(k)\vec{\sigma}(k). \qquad (49)$$

We have introduced the spherical components t_μ of the isospin single-particle operator and used the bare weak charges $g_v = 1$ and $g_A = 1.25$.

In both ^{17}O and ^{17}F, the magnetic moments are practically determined at the HF level (Table V). The weak quenching due to the core brings the total moments slightly more distant from the experimental values. It may be worth to point out that the core contribution originates from the spin-flip partners present in the HF p-h configurations entering the TDA phonons and, therefore, is ultimately ascribed to HF.

The β decay is also ruled by HF. Indeed, the ft value comes almost entirely from the transition between the HF components of the ^{17}O and ^{17}F $5/2_1^+$ ground states (Table V). The weak quenching caused by the phonon coupling brings the ft value slightly above the measured quantity.

B. Electric quadrupole moments and low-lying transitions

We used the electric multipole operator

$$\mathcal{M}(E\lambda\mu) = \sum_i e_i r_i^\lambda Y_{\lambda\mu}(\hat{r}_i) \qquad (50)$$

for $\lambda = 2$ with bare charges $e_i = e$ for protons and $e_i = 0$ for neutrons.

In ^{17}O, the calculation underestimates the absolute value of the ground-state quadrupole moment by a factor three and the strength of the transition from the ground state $5/2_1^+$ to $1/2_1^+$ by an order of magnitude (Table V).

Since $5/2_1^+$ and $1/2_1^+$ have a prominent single-particle character (Table I) and the odd particle is a neutron ($e_k = 0$),
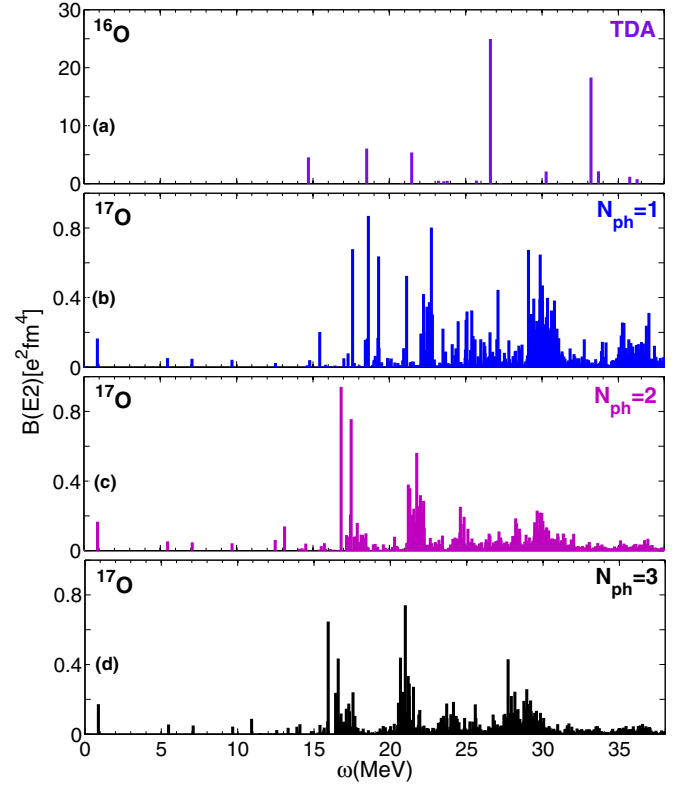
FIG. 3. $E2$ strength distribution of ^{17}O computed in spaces including up to (b) $N_{ph} = 1$, (c) $N_{ph} = 2$, and (d) $N_{ph} = 3$ phonons. The TDA spectrum of (a) ^{16}O is also shown for comparison. A different scale is used for the latter plot.

the contribution to the moment and transition strength comes entirely from the terms $\mathcal{M}_{01}(E2)$ [Eq. (25)] and $\mathcal{M}_{10}(E2)$ [Eq. (26)] coupling the single-particle components of $5/2_1^+$ and $1/2_1^+$ to the $\lambda = 2^+$ particle-phonon pieces of $1/2_1^+$ and $5/2_1^+$, respectively.

As shown in Table I, the one-phonon terms account for $\sim 5\%$ of $|\Psi_{5/2_1^+}\rangle$ and $\sim 6\%$ of $|\Psi_{1/2_1^+}\rangle$. The quadrupole phonon content of $|\Psi_{5/2_1^+}\rangle$ and $|\Psi_{1/2_1^+}\rangle$ is $W_{2^+} \sim 0.8\%$ and $W_{2^+} \sim 1.2\%$, respectively (Table II). The specific components $|(5/2_i^+ \times 2_k^+)^{5/2}\rangle$ and $|(1/2_i^+ \times 2_k^+)^{5/2}\rangle$, responsible for the quadrupole moment and the $E2$ transition, are present in the state $|\Psi_{5/2_1^+}\rangle$ with weights (43) $W_{5/2^+2^+} \sim 0.2\%$ and $W_{1/2^+2^+} \sim 0.3\%$, respectively, while $|(5/2_i^+ \times 2_k^+)^{1/2}\rangle$ represent $\sim 0.7\%$ of $|\Psi_{1/2_1^+}\rangle$.

It seems, therefore, that the amplitudes of the one-phonon components and, in particular, the quadrupole phonon pieces are not sufficiently large. Indeed, as shown in Fig. 3(a), all the 2^+ TDA states are above ~ 15 MeV, and those collecting most of the strength are above ~ 25 MeV. It is, therefore, natural to expect that quadrupole phonons of such high energies get admixed weakly with the low-energy single-particle states. In fact, when the odd neutron is coupled to the multiphonon core components, the $E2$ strength gets highly fragmented but remains concentrated at high energy. It is, therefore, necessary to include four-phonon states. As pointed out already, in fact, only these configurations would push down the two-phonon

components thereby favoring a more effective particle-phonon and phonon-phonon mixing.

In ^{17}F, the quadrupole moment, computed in HF, is $\sim$1.7 times the measured value. It gets considerably smaller and closer to experiments once the phonon coupling is included. This coupling is even more effective on the $5/2_1^+ \rightarrow 1/2_1^+$ $E2$ transition. Once the phonons are included, in fact, the $E2$ strength, which is $\sim$1.8 times larger in HF, is drastically reduced and coincides in practice with the experimental value (Table V).

The strong quenching action of the phonon coupling in ^{17}F seems to clash with the analysis just made for the ^{17}O, especially since the HF components of $5/2_1^+$ and $1/2_1^+$ in ^{17}F are even more dominant than in ^{17}O (Table III). The one-phonon piece represents only the $\sim$3.5% and $\sim$3.2% of $|\Psi_{5/2_1^+}\rangle$ and $|\Psi_{1/2_1^+}\rangle$, respectively. The contribution of the quadrupole configurations $|[5/2_i^+ \times 2_k^+]^{5/2}\rangle$ and $|(1/2_i^+ \times 2_k^+)^{5/2}\rangle$ to $|\Psi_{5/2_1^+}\rangle$ amounts to $\sim$0.2% and $\sim$0.1%, respectively, while the $|(5/2_i^+ \times 2_k^+)^{1/2}\rangle$ accounts for $\sim$0.4% of $|\Psi_{1/2_1^+}\rangle$.

The contradiction, however, is only apparent. In fact, the phonons exert a twofold action. They not only get admixed directly with the HF components, but combine the HF states among themselves. In fact, the single-particle piece of each wave function $|\Psi_\nu\rangle$ is a linear combination of different HF configurations. Their mutual interference causes the quenching of quadrupole moment and transition in ^{17}F. In ^{17}O, this interference has no effect since the odd neutron carries no charge.

C. Low-lying electric-dipole transitions

For the $E1$ transitions we use the intrinsic operator referred to the c.m. coordinate. This keeps the form (50) for $\lambda = 1$ with effective charges $e_i = (N/A)e$ for protons and $e_i = -(Z/A)e$ for neutrons.

The effective charges do not affect the TDA core states, which are free of c.m. spurious admixtures in virtue of the orthogonalization method outlined already. It modifies, instead, the single-particle contributions, especially the transitions between states of dominant single-particle character. This contribution was ignored in computing the dipole cross section in Ref. [27]. As we shall see, however, the changes induced by the effective charges affect the cross section only in the low-energy sector and do not invalidate any of the conclusions drawn in Ref. [27].

1. ^{17}O

As shown in Table V, the $5/2_1^+ \rightarrow 5/2_1^-$ $E1$ reduced strength, although small, is an order of magnitude larger than the experimental value (Table V). The EMPM $5/2_1^-$ state involved in the transition is an intruder bearing no relation to the corresponding HF state. As shown in Table I, it has a very small single-particle content and a dominant particle-phonon component. Thus, the strength comes entirely from the core excitation. We have, in fact, $\mathcal{M}_{00}(E1) = 0.0008efm$, $\mathcal{M}_{01}(E1) = 0.1587efm$, and $\mathcal{M}_{10}(E1) = 0.00003efm$. The overestimation of the experimental strength suggests that the amplitude of the particle-phonon component of the EMPM $5/2_1^-$ is too large.

The $E1$ transition from $1/2_1^+$ to $1/2_1^-$, both of single-particle nature (Table I), carries a strength three orders of magnitude larger than the very small experimental quantity. This, instead, is reproduced by the strength of the transition to the second $1/2_2^-$ at 8.47 MeV with dominant one-phonon components (Table I). It would be, therefore, tempting to associate this latter state to the first experimental $1/2^-$, were not for its too high energy, three times larger. To test the validity of such a suggestion, one should check if more effective particle-phonon and phonon-phonon couplings, advocated by the analysis of energy levels and quadrupole transitions, are able to produce an energy crossing between $1/2_2^-$ at 8.47 MeV and $1/2_1^-$ at 5.26 MeV.

On the ground of the present results, we can only state that the the $1/2_1^+ \rightarrow 1/2_1^-$ transition, like other transitions of single-particle nature we will encounter in both ^{17}O and ^{17}F, carry an unrealistically large $E1$ strength.

2. ^{17}F

The $5/2_1^+ \rightarrow 5/2_1^-$ $E1$ theoretical reduced strength is about half of the experimental value (Table III) and is the outcome of a partial cancellation between the single-particle $[\mathcal{M}_{00}(E1) = -0.039efm]$ and the particle-phonon $[\mathcal{M}_{01}(E1) = 0.020efm$ and $\mathcal{M}_{10}(E1) = 0.001efm]$ contributions. It is to be noticed that the single-particle contribution, which is negligible in ^{17}O, is comparable to the one induced by the core excitation in ^{17}F. The reason for such a difference is due to the larger amplitudes of the single-particle components of both $5/2_1^+$ and $5/2_1^-$ in ^{17}F (Table III) with respect to ^{17}O (Table I).

The $1/2_1^+ \rightarrow 1/2_1^-$ $E1$ transition strength is overestimated by three orders of magnitude, just like in ^{17}O. This unrealistically large value comes entirely from the transition between the single-particle components of the two states $[\mathcal{M}_{00}(E1) = 0.900efm]$. The core terms are much smaller and of opposite sign $[\mathcal{M}_{01}(E1) = 0.017efm$ and $\mathcal{M}_{10}(E1) = -0.012efm]$. This is another example of a single-particle transition carrying an unrealistically large strength.

A strength comparable to the experimental one is collected by the $1/2_3^-$ (Table V). This state lies at 10.19 MeV, about three times the experimental value but, unlike the $1/2_2^-$ in ^{17}O, is a linear combination of single-particle and one-phonon components of comparable amplitudes (Table III). It would be plausible to associate such a state to the lowest experimental $1/2^-$ level, if a crossing between the $1/2_3^-$ and $1/2_1^-$ levels could be achieved by a stronger particle-phonon coupling.

D. Electric-dipole spectra and cross sections

We computed the dipole cross section

$$\sigma = \int_0^\infty \sigma(\omega)d\omega = \frac{16\pi^3}{9\hbar c} \int_0^\infty \omega \mathcal{S}(E1,\omega)d\omega, \quad (51)$$

where $\mathcal{S}(E1,\omega)$ is the strength function

$$\mathcal{S}(E1,\omega) = \sum_\nu B_\nu(E1)\delta(\omega - \omega_\nu)$$

$$\approx \sum_\nu B_\nu(E1)\rho_\Delta(\omega - \omega_\nu). \quad (52)$$
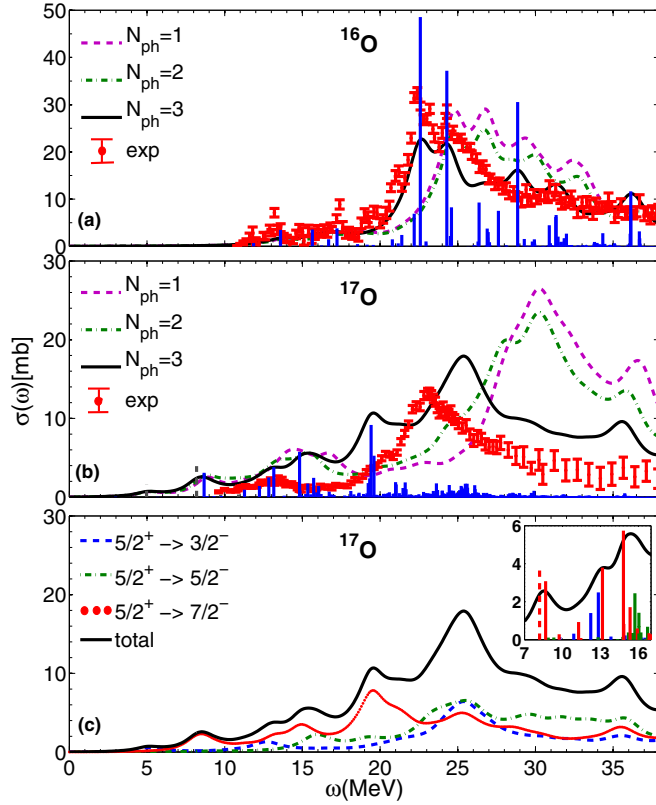
FIG. 4. The theoretical $E1$ cross sections, computed in different multiphonon spaces, are compared with the experimental ones in (a) ^{16}O and (b) ^{17}O. The data are taken from Ref. [41] for ^{16}O and from Ref. [42] for ^{17}O. A Lorentzian of width $\Delta = 2$ MeV is used. The dashed bars denote the transitions of single-particle character. The separate contributions of the $3/2_i^-$, $5/2_i^-$, and $7/2_i^-$ excitations to the $E1$ cross section in ^{17}O are shown in panel (c). The red bars in the inset refer to the $5/2^+ \rightarrow 7/2^-$ transitions.

Here ω is the energy variable, $B_\nu(E1)$ is the reduced strength of the transition to the ν_{th} excited state of energy $\omega_\nu = \mathcal{E}_\nu - \mathcal{E}_{\nu_0}$, and

$$\rho_\Delta(\omega - \omega_\nu) = \frac{\Delta}{2\pi} \frac{1}{(\omega - \omega_\nu)^2 + \left(\frac{\Delta}{2}\right)^2} \quad (53)$$

is a Lorentzian of width Δ, which replaces the δ function as a weight of the reduced strength.

After integration, the cross section becomes

$$\sigma(E1) = \frac{16\pi^3}{9\hbar c} m_1(E1), \quad (54)$$

where

$$m_1(E1) = \sum_\nu \omega_\nu B_\nu(E1) \quad (55)$$

is the first moment.

If the Hamiltonian does not contain momentum-dependent and exchange terms, m_1 fulfills the classical energy weighted Thomas–Reiche–Kuhn (TRK) sum rule

$$m_1(E1) = \frac{\hbar^2}{2m} \frac{9}{4\pi} \frac{NZ}{A} e^2, \quad (56)$$
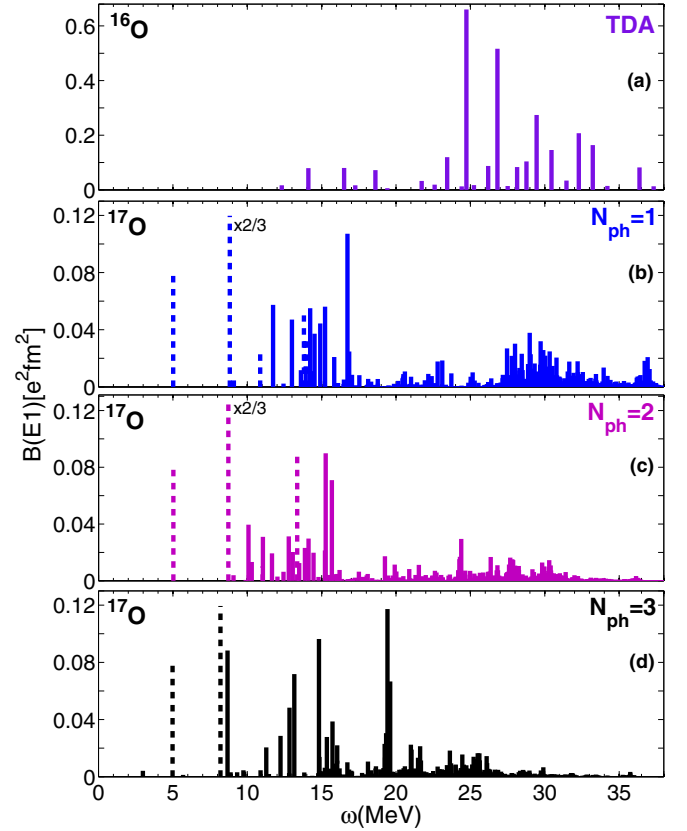
FIG. 5. $E1$ strength distribution of ^{17}O computed in spaces including up to (b) $N_{ph} = 1$, (c) $N_{ph} = 2$, and (d) $N_{ph} = 3$ phonons. The TDA spectrum of (a) ^{16}O is also shown for comparison. A different scale is used for the latter plot. The dashed bars indicate the transitions of single-particle nature.

and the total cross section assumes the value

$$\sigma(E1) = (2\pi)^2 \frac{\hbar^2}{2m} \frac{e^2}{\hbar c} \frac{NZ}{A} = 60 \frac{NZ}{A} (\text{MeV mb}). \quad (57)$$

1. Dipole response in ^{16}O

We start with investigating the dipole response in ^{16}O. As shown in Fig. 4(a), the TDA cross section is displaced slightly upward in energy with respect to experiments. The action of the two phonons is weak. The three phonons, instead, strongly affect the cross section, which gets shifted downward and peaked in the right position. They have also a damping action which shortens the height of the peaks. The shape of the cross section is not so distant from that resulting from the measurements. The two main peaks, for instance, are reproduced fairly well. Each of them arises mainly from a strong transition to a single TDA state. The other secondary peaks are also due mainly to single transitions.

2. Dipole response in ^{17}O

In ^{17}O, the cross section gets displaced upward in energy by the coupling of the odd particle to the TDA phonons. Its main peak is too high and lies several MeV above the experimental one [Fig. 4(b)]. As in ^{16}O, the cross section gets damped and
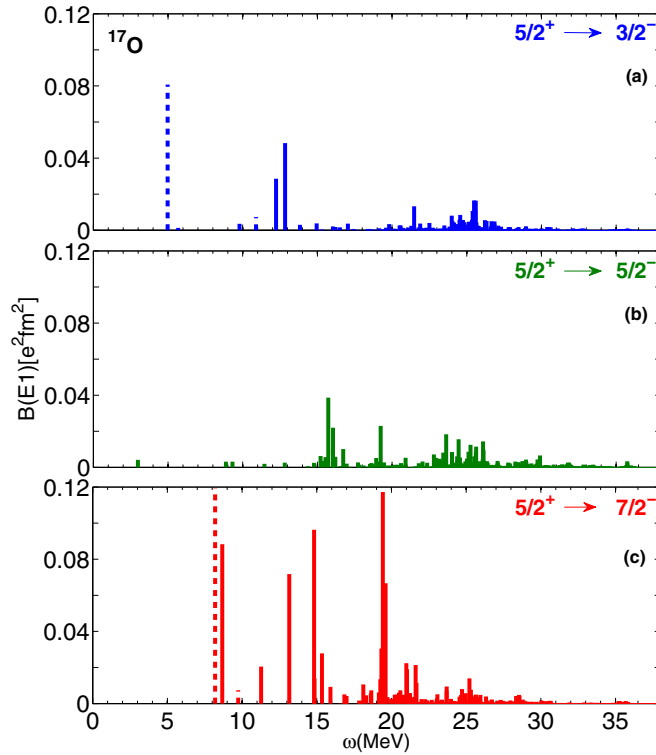
FIG. 6. $E1$ strength distribution of the transitions to (a) $3/2_i^-$, (b) $5/2_i^-$, and (c) $7/2_i^-$ in ^{17}O. The dashed bars indicate the transitions of single-particle nature.

TABLE VI. Contributions of the TDA 1^- phonons and their weights $P^{\nu'}$ [Eq. (28)] to the strengths of the strongest $E1$ transitions in ^{17}O. W [Eq. (42)] gives the weight of the 1^- phonons in the final states $|\Psi_{\nu'}\rangle$. The energies ω are in MeV and the $B(E1)$ in e^2 fm^2.

$\nu' = 3/2_6^-$	$\omega_{\nu'} = 12.83$	$W_{1^-}^{\nu'} = 0.091$	$B_{\nu'}(E1) = 0.032$
λ_k	ω_{λ_k}	$\mathcal{M}_{\lambda_k}$	$P^{\nu'}_{p\lambda_k}$	$\mathcal{M} \times P$
1_5^-	18.61	0.155	−0.249	−0.039
1_{11}^-	24.73	−0.469	0.152	−0.071
1_{13}^-	26.20	0.171	−0.163	−0.028
1_{14}^-	26.82	−0.415	0.208	−0.086
1_{17}^-	28.77	0.186	−0.212	−0.040
1_{19}^-	30.45	−0.221	0.183	−0.040
1_{21}^-	32.29	0.263	−0.110	−0.029
1_{22}^-	33.23	−0.234	0.094	−0.022

$\nu' = 5/2_{13}^-$	$\omega_{\nu'} = 16.04$	$W_{1^-}^{\nu'} = 0.078$	$B(E1) = 0.037$
λ_k	ω_{λ_k}	$\mathcal{M}_{\lambda_k}$	$P^{\nu'}_{p\lambda_k}$	$\mathcal{M} \times P$
1_2^-	14.11	0.163	−0.319	−0.052
1_5^-	18.61	0.155	−0.588	−0.091
1_{11}^-	24.73	−0.469	0.195	−0.091
1_{14}^-	26.82	−0.415	0.204	−0.085
1_{22}^-	33.23	−0.234	0.173	−0.040

$\nu' = 7/2_{29}^-$	$\omega_{\nu'} = 19.33$	$W_{1^-}^{\nu'} = 0.061$	$B(E1) = 0.129$
λ_k	ω_{λ_k}	$\mathcal{M}_{\lambda_k}$	$P^{\nu'}_{p\lambda_k}$	$\mathcal{M} \times P$
1_3^-	16.51	−0.163	−0.318	0.052
1_5^-	18.61	0.155	0.767	0.119
1_9^-	23.44	−0.200	−0.200	0.040
1_{11}^-	24.73	−0.469	−0.136	0.064
1_{13}^-	26.19	0.171	0.184	0.031
1_{14}^-	26.82	−0.415	−0.303	0.126
1_{17}^-	28.77	0.186	0.231	0.043
1_{18}^-	29.45	−0.302	−0.567	0.171
1_{19}^-	30.45	−0.221	−0.350	0.077
1_{22}^-	33.23	−0.234	−0.276	0.065

down-shifted mainly by the couplings to three phonons. The peak, however, is still too high and ~2 MeV above in energy.

A better understanding of the excitation mechanism is gained by investigating the strength distribution. From comparing the TDA spectrum of ^{16}O [Fig. 5(a)] with the corresponding one in ^{17}O [Fig. 5(b)] one notices that adding an odd particle to the core induces a huge damping and fragmentation. Such an effect was largely expected, since the strength collected by each 1^- core state gets distributed among several states of spin $3/2^-$, $5/2^-$, and $7/2^-$ (Fig. 6).

The coupling to two phonons induces an appreciable damping over the whole spectrum, especially in the high-energy sector [Fig. 5(c)]. The three phonons deplete almost completely the high-energy region and pack most of the strength in the range 5–25 MeV [Fig. 5(d)]. This is the outcome of two actions. The three phonons shift the one-phonon energies downward and strengthen the amplitudes of several one-phonon states at the expenses of the two phonons.

The main peak of the theoretical cross section [Fig. 4(b)] arises from a bunch of closely packed weakly excited levels around ~25 MeV. As the plots in Fig. 6 show, all three $3/2^-$, $5/2^-$, and $7/2^-$ states carry strength in this region (Fig. 6) and, therefore, contribute to the main peak on equal footing [Fig. 4(c)].

The unwanted secondary peak at ~20 MeV [Fig. 4(b)] originates mostly from the strong transitions to the $7/2^-$ states at the same energy [Fig. 6(c)]. At low energy, we can distinguish four small humps [Fig. 4(c)]. The small one at ~5 MeV comes from the excitation of the single-particle $3/2_1^-$

state [Fig. 6(a)], the one within 5–10 MeV is due to the two $7/2^-$ states at ~8 MeV [Fig. 6(c)], the lowest one being of single-particle nature. Also the two peaks around ~12.5 MeV and ~15 MeV arise mostly from exciting a few $7/2^-$ states [inset of Fig. 4 (c)] with a small contribution of $3/2^-$ states [Fig. 6(a)] to the first peak and of $5/2^-$ excitations [Fig. 6(b)] to the second.

It is clear from the above analysis that the transitions of single-particle character affect shape and magnitude of the low-energy queue of the cross section. They are the analogs of the too strong $1/2_1^+ \rightarrow 1/2_1^-$ transition discussed above (Table V) and, therefore, are likely to carry unrealistically large strengths. Without their contribution, the small peak at ~5 MeV would disappear and the low-energy trend of the cross section would be smoother [27].

Important differences between ^{16}O and ^{17}O emerge also from the analysis of the integrated cross section. The experimental cross section integrated up to 40 MeV over-exhausts the TRK sum rule by a factor ~1.26 in ^{16}O, to be compared with the computed fraction of ~100%. In ^{17}O, the theoretical integrated cross section accounts for ~98% of the TRK sum rule, while the fraction exhausted by the data is ~50%. An
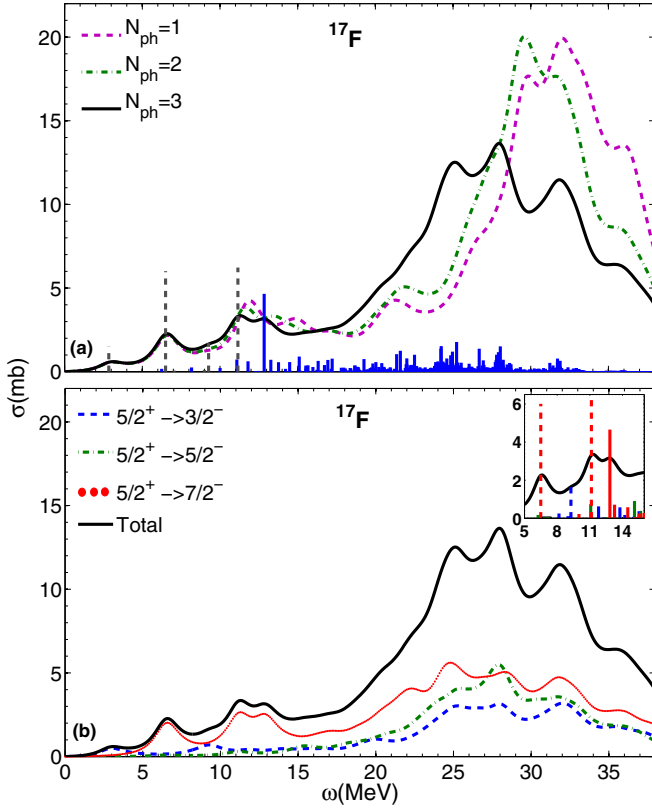
FIG. 7. (a) The theoretical $E1$ cross sections, computed in different multiphonon spaces, are plotted for ^{17}F. A Lorentzian of width $\Delta = 2$ MeV is used. The separate contributions of the $3/2_i^-$, $5/2_i^-$, and $7/2_i^-$ excitations are shown in panel (b). The red bars in the inset refer to the $5/2^+ \rightarrow 7/2^-$ transitions. The dashed bars indicate the transitions of single-particle character.

FIG. 8. $E1$ strength distribution of ^{17}F computed in spaces including up to (a) $N_{ph} = 1$, (b) $N_{ph} = 2$, and (c) $N_{ph} = 3$ phonons. The dashed bars indicate the transitions of single-particle nature.

appreciable share goes to the region of the pygmy resonance. The strength integrated up to $\omega \lesssim 15$ MeV exhausts $\sim 9\%$ of the TRK sum rule, three times the measured value $\sim 3.2\%$. Had we ignored the single-particle contribution, the computed fractions would have been $\sim 91\%$ and, for the pygmy, $\sim 3.5\%$ [27].

The analysis of the phonon structure of the states involved in the transitions may contribute to clarify why the calculation yields a too large cross section. We have pointed out already that the single-particle levels carry too large strength. They are very few and lie at low energy. The other states $\Psi_{\nu'}$ are linear combinations of dominant one-phonon components and two and three phonons. The one-phonon weights cluster around $\sim 65\%$, and the shares W of the dipole configurations $|[5/2_i^+ \times (1_k^-)]^{\nu}\rangle$ ($\nu = 3/2^-$, $5/2^-$, $7/2^-$) range from $\sim 5\%$ to $\sim 15\%$. These amplitudes would be reduced by a stronger admixing with the particle and the other n-phonon components.

The strengths are determined by the joint contribution of the $\lambda = 1$ TDA phonon amplitudes $\mathcal{M}_{1_k^-}$ and the weights $P_{p1_k^-}^{(\nu')}$ [Eq. (28)], incorporating the structural composition of $\Psi_{\nu'}$. How the different phonons contribute to the strengths is illustrated in Table VI for a few selected transitions.

The table also shows that the transitions are not determined by a single collective 1^- state. Several dipole phonons contribute on equal footing. Moreover, the strength collected by a given 1^- phonon gets distributed among several dipole transitions in ^{17}O thereby determining the huge fragmentation we discussed already.

3. Dipole response in ^{17}F

The phonon action in ^{17}F is analogous to the one exerted in ^{17}O. The cross section gets quenched and shifted mainly by the coupling to three phonons [Fig. 7(a)]. Its behavior is smoother than in ^{17}O. We get, in fact, a broad wiggly hump, covering a wide energy range (20–40 MeV), which arises from a huge number of closely packed small peaks.

The cross sections coming separately from the excitations of $3/2_i^-$, $5/2_i^-$, and $7/2_i^-$ states all have the same trend [Fig. 7(b)] over the whole energy range covered by the hump.

The spectrum in Fig. 7(a) shows that the fragmentation is astonishingly large. It is mainly induced by the coupling of the odd proton to the TDA phonons [Fig. 8(a)] and further enhanced by two and, especially, three phonons [Figs. 8(b) and 8(c)]. Strong transitions are predicted only at energies $\lesssim 15$ MeV [Fig. 8(c)]. The lowest four are due to single-particle excitations and yield the lowest three humps in the cross section (Fig. 7). They are the analogs of the $1/2_1^+ \rightarrow 1/2_1^-$

transition discussed above (Table V) and, like this, carry unrealistically large strengths.

The fourth hump in the 13–15 MeV interval arises almost entirely from the excitation of $7/2_3^-$ with small contributions of other weak transitions, including $5/2_1^+ \rightarrow 7/2_4^-$ [inset of Fig. 7(b)]. It is likely to correspond to the pygmy resonance, which, according to the experimental analysis of Ref. [39], is due to the excitation of two $7/2^-$ states, accounting for $\sim$2% of the TRK sum rule. The integrated cross section up to $\sim$40 MeV exhausts $\sim$81% of the same sum.

The final states $\Psi_{\nu'}$ have a structure quite similar to the one obtained for ^{17}O. Except for the four low-lying states of single-particle character, they have a multiphonon nature with dominant one-phonon components. The weights of $|\nu_1\rangle$ are concentrated around $\sim$65% and those of the dipole configurations $|[5/2_i^+ \times (1_k^-)]^\nu\rangle$ ($\nu = 3/2^-, 5/2^-, 7/2^-$) range from $\sim$5% to $\sim$15%.

VI. CONCLUDING REMARKS

Let us summarize the main results of our calculation. Concerning the energy spectra, (i) the one-phonon states improve the description of the low-lying positive-parity levels of single-particle character through their coupling, but remain too high in energy; (ii) the two phonons do not alter the low energy levels, couple weakly with the one-phonon states, and mix only with those of comparable energies in the high-energy region; (iii) the three phonons couple strongly to the negative-parity one-phonon states and push a few of them into the low-energy sector; (iv) they affect marginally the positive-parity one-phonon and the two-phonon states. The overall result is that the calculation is far from reproducing the high density of the experimental level scheme at low energy.

As for moments and transitions, (i) the phonon coupling has a very weak quenching effect on magnetic moments and ft values, practically determined by the HF components; (ii) the core corrections to the ground-state quadrupole moments and to the $E2$ transitions between low-lying states, of single-particle nature, are substantial but not sufficient to bring the mentioned observables close to the experimental values; (iii) a few low-lying $E1$ transitions have single-particle nature and carry unrealistically large strengths; (iv) most of the $E1$ transitions and resonances are determined by the particle-core states with dominant one-phonon components; (v) the damping and energy shift induced by the coupling to two and three phonons are appreciable but not sufficient to reproduce the peak and shape of the cross section in ^{17}O. Its magnitude is also largely overestimated.

A detailed analysis of the phonon structure of the wave functions indicates that all discrepancies between theory and experiments originate from an insufficient particle-phonon and phonon-phonon admixture. In particular, the one-phonon components have too small weights in the states of dominant single-particle character, lying generally at low energies, and too large amplitudes in the dominantly particle-core states.

This insufficient admixing might be traced back to HF. In both ^{17}O and ^{17}F, the levels or groups of levels above the Fermi surface are too far apart, especially as the energy increases

(Figs. 1 and 2), a common feature of HF spectra derived from NN interactions [40,43,44]. These gaps are reduced substantially but not completely by the phonon coupling.

It is, therefore, desirable to investigate if it is possible to obtain a smoother HF level scheme by a refinement of the NNLO$_{opt}$ potential or by adopting other versions of chiral potential like the NNLO$_{sat}$ [45], which includes explicitly the three-body contribution and improves the description of binding energies and nuclear radii as well [46]. A more compressed HF spectrum would yield more closely packed TDA phonons and, therefore, might enhance the coupling of the one-phonon components to the HF vacuum and to the other n-phonon states.

The positive-parity states would be marginally affected by a more accurate HF level scheme, unless we include the four-phonon states which are expected to couple strongly to the two-phonons, on the ground of the heuristic argument given in Sec. IV A. In particular, the coupling should be more effective among the components of positive parity, which have the lowest energies. Thus, the positive-parity two-phonon states lying just above $\sim$16 MeV are likely to be pushed down in energy and to mix strongly with the low-lying one-phonon components above $\sim$11 MeV.

The presence of (2p-2h) and, even (4p-4h) positive-parity levels at low energy in ^{16}O was predicted long ago in the pioneering work of Brown and Green [47] and ascertained quantitatively by a phenomenological shell-model calculation [48].

It is, therefore, mandatory to include at least four phonons for a satisfactory description of the full energy spectra and transitions in the two nuclei investigated here. Including four phonons is a difficult but not impossible task if we are allowed to resort to approximations analogous to those we made here for three phonons.

The present calculation illustrates exhaustively the potential of the EMPM. The particle-phonon structure has allowed us to incorporate configurations of increasing complexity up to arbitrarily high energies and, therefore, to perform large-scale, parameter-free, self-consistent calculations starting from bare NN forces. Having all wave functions at our disposal, we could investigate their phonon composition and, therefore, clarify how the different n-phonon states of each multipolarity act selectively on the different observables. Such a detailed investigation has also suggested reliable recipes for curing the discrepancies between theory and experiments.

[1] A. Bohr and B. R. Mottelson, *Nuclear Structure* (W. A. Benjamin, New York, 1975), Vol II.

[2] C. Mahaux, P. F. Bortignon, R. A. Broglia, and C. H. Dasso, Phys. Rep. **120**, 1 (1985).

[3] K. Yoshida, Phys. Rev. C **79**, 054303 (2009).

[4] G. Colò, H. Sagawa, and P. Bortignon, Phys. Rev. C **82**, 064307 (2010).

[5] P. F. Bortignon, G. Colò, and H. Sagawa, J. Phys. G **37**, 064013 (2010).

[6] K. Mizuyama, G. Colò, and E. Vigezzi, Phys. Rev. C **86**, 034318 (2012).

[7] L.-G. Cao, G. Colò, H. Sagawa, and P. F. Bortignon, Phys. Rev. C **89**, 044314 (2014).

[8] D. Tarpanov, J. Dobaczewski, J. Toivanen, and B. G. Carlsson, Phys. Rev. Lett. **113**, 252501 (2014).

[9] M. Baldo, P. F. Bortignon, G. Colò, D. Rizzo, and L. Sciacchitano, J. Phys. G **42**, 085109 (2015).

[10] G. Co', V. De Donno, M. Anguiano, R. N. Bernard, and A. M. Lallena, Phys. Rev. C **92**, 024314 (2015).

[11] N. V. Gnezdilov, I. N. Borzov, E. E. Saperstein, and S. V. Tolokonnikov, Phys. Rev. C **89**, 034304 (2014).

[12] E. Litvinova and P. Ring, Phys. Rev. C **73**, 044328 (2006).

[13] E. V. Litvinova and A. V. Afanasjev, Phys. Rev. C **84**, 014305 (2011).

[14] E. Litvinova, Phys. Rev. C **85**, 021303(R) (2012).

[15] A. V. Afanasjev and E. Litvinova, Phys. Rev. C **92**, 044317 (2015).

[16] J. Toivanen and J. Suhonen, Phys. Rev. C **57**, 1237 (1998).

[17] S. Mishev and V. V. Voronov, Phys. Rev. C **78**, 024310 (2008).

[18] M. Tohyama and P. Schuck, Phys. Rev. C **87**, 044316 (2013).

[19] J. R. Gour, P. Piecuch, M. Hjorth-Jensen, M. Wloch, and D. J. Dean, Phys. Rev. C **74**, 024310 (2006).

[20] G. Hagen, T. Papenbrock, and M. Hjorth-Jensen, Phys. Rev. Lett. **104**, 182501 (2010).

[21] G. Hagen, M. Hjorth-Jensen, G. R. Jansen, R. Machleidt, and T. Papenbrock, Phys. Rev. Lett. **108**, 242501 (2012).

[22] G. R. Jansen, J. Engel, G. Hagen, P. Navratil, and A. Signoracci, Phys. Rev. Lett. **113**, 142502 (2014).

[23] G. Hagen, T. Papenbrock, M. Hjorth-Jensen, and D. J. Dean, Rep. Prog. Phys. **77**, 096302 (2014).

[24] A. Cipollone, C. Barbieri,, and P. Navrátil, Phys. Rev. Lett. **111**, 062501 (2013).

[25] B. R. Barrett, P. Navrátil, and J. P. Vary, Prog. Part. Nucl. Phys. **69**, 131 (2013).

[26] J. D. Holt, J. Menéndez, and A. Schwenk, Eur. Phys. J. A **49**, 39 (2013).

[27] G. De Gregorio, F. Knapp, N. Lo Iudice, and P. Veselý, Phys. Rev. C **94**, 061301(R) (2016).

[28] F. Andreozzi, F. Knapp, N. Lo Iudice, A. Porrino, and J. Kvasil, Phys. Rev. C **75**, 044312 (2007).

[29] F. Andreozzi, F. Knapp, N. Lo Iudice, A. Porrino, and J. Kvasil, Phys. Rev. C **78**, 054308 (2008).

[30] D. Bianco, F. Knapp, N. Lo Iudice, F. Andreozzi, and A. Porrino, Phys. Rev. C **85**, 014313 (2012).

[31] D. Bianco, F. Knapp, N. Lo Iudice, F. Andreozzi, A. Porrino, and P. Veselý, Phys. Rev. C **86**, 044327 (2012).

[32] F. Knapp, N. Lo Iudice, P. Veselý, F. Andreozzi, G. De Gregorio, and A. Porrino, Phys. Rev. C **90**, 014310 (2014).

[33] F. Knapp, N. Lo Iudice, P. Veselý, F. Andreozzi, G. De Gregorio, and A. Porrino, Phys. Rev. C **92**, 054315 (2015).

[34] G. De Gregorio, F. Knapp, N. Lo Iudice, and P. Veselý, Phys. Rev. C **93**, 044314 (2016).

[35] K. Bennaceur, F. Nowacki, J. Okolowicz, and M. Ploszajczak, Nucl. Phys. A **671**, 203 (2000).

[36] E. K. Warburton and B. A. Brown, Phys. Rev. C **46**, 923 (1992).

[37] H. Sagawa and T. Suzuki, Nucl. Phys. A **687**, 111 (2001).

[38] A. Ekström, G. Baardsen, C. Forssén, G. Hagen, M. Hjorth-Jensen, G. R. Jansen, R. Machleidt, W. Nazarewicz, T. Papenbrock, J. Sarich *et al.*, Phys. Rev. Lett. **110**, 192502 (2013).

[39] D. Tilley, H. Weller, and C. Cheves, Nucl. Phys. A **564**, 1 (1993).

[40] D. Bianco, F. Knapp, N. Lo Iudice, P. Veselý, F. Andreozzi, G. De Gregorio, and A. Porrino, J. Phys. G **41**, 025109 (2014).

[41] J. Ahrens, H. Borchert, K. Czock, H. Eppler, H. Gimm, H. Gundrum, M. Krning, P. Riehn, G. S. Ram, A. Zieger *et al.*, Nucl. Phys. A **251**, 479 (1975).

[42] J. W. Jury, B. L. Berman, D. D. Faul, P. Meyer, and J. G. Woodworth, Phys. Rev. C **21**, 503 (1980).

[43] R. Roth, P. Papakonstantinou, N. Paar, H. Hergert, T. Neff, and H. Feldmeier, Phys. Rev. C **73**, 044312 (2006).

[44] H. Hergert, P. Papakonstantinou, and R. Roth, Phys. Rev. C **83**, 064317 (2011).

[45] A. Ekström, G. R. Jansen, K. A. Wendt, G. Hagen, T. Papenbrock, B. D. Carlsson, C. Forssén, M. Hjorth-Jensen, P. Navrátil, and W. Nazarewicz, Phys. Rev. C **91**, 051301 (2015).

[46] V. Lapoux, V. Somà, C. Barbieri, H. Hergert, S. R. Holt, and J. D. Stroberg, Phys. Rev. Lett. **117**, 052501 (2016).

[47] G. E. Brown and A. M. Green, Nucl. Phys. **75**, 401 (1966).

[48] W. C. Haxton and C. Johnson, Phys. Rev. Lett. **65**, 1325 (1990).